Int. J. Electrochem. Sci., 12 **(2017)** 7326 – 7340, doi: 10.20964/2017.08.36

International Journal of
ELECTROCHEMICAL
SCIENCE
www.electrochemsci.org

Facile Preparation of Highly Porous Carbon from Bean Dregs for Enhanced Electrochemical Performance

Yan YANG[1], *Jianhua ZHA*[1], *Liang LIU*[2], *Ningyi YUAN*[1,*]

[1] Jiangsu Collaborative Innovation Center of Photovoltaic Science and Engineering, Changzhou Jiangsu, 213000, China;
[2] School of Environmental and Safety Engineering, Changzhou University, Changzhou Jiangsu, 213000;
[*]E-mail: eihezuo@163.com

Received: 6 May 2017 / *Accepted:* 11 June 2017 / *Published:* 12 July 2017

In this work, we propose a cost-effective method to convert bean dregs to high-performance porous carbon as supercapacitor electrode materials. We implement an activation process with KOH to induce well-developed porous structure to achieve a high specific surface area (up to 3104 m^2 g^{-1}) and high specific capacitance (up to 268 F g^{-1}), indicating superior electrochemical properties. We also investigate how the key parameters, in terms of activation temperature, time and ratio, determine the pore structures and electrochemical properties. In addition, the porous carbon produced from our method may serve great potential for multi-disciplined fields such as separation, catalysis and hydrogen storage.

Keywords: biomass; bean dreg; porous carbon; activation; supercapacitors

1. INTRODUCTION

With the gradual depletion of fossil-based resources and increasing concerns about the environmental pollution, research and development in renewable energy and resources with high environmental benignity and sustainability has become a global interest. Biomass is one of the most abundant and highly developed renewable resources, which refers to any renewable or recycled organic matter that can be converted into energy materials with huge benefits in environmental friendliness and commercial gain[1]. More importantly, as the sole carbon source in renewable resources, biomass is an important precursor to produce high-performance carbonaceous material with well-controlled microstructure, drawing worldwide attention[2]. Among all carbonaceous materials, porous carbon is very promising due to its well-developed pores, high surface area, low density, high

thermal conductivity, excellent chemical and mechanical stability, and good electrical conductivity[3]. Porous carbon has been applied in a wide range of areas, such as catalytic[4], hydrogen storage[5], biomedical[6], water treatment[7] and capacitors[8] with great practical prospects.

Supercapacitors (SCs) has recently received considerable attention as a renewable energy source, because of their high power density, fast charge/discharge capability, long life cycle, and the combined advantages of both batteries and dielectric capacitors to store massive energy and deliver high power in a very short time[9]. Commercial SCs are mainly electrical double layer capacitor (EDLCs), which accumulate charges at the interface between the electrode and the electrolyte to form an electrical double layer with a service life of thousands of cycles[10]. The porous carbon electrode material is considered to be the best choice of EDLCs with the key advantages of low cost, high surface area and high specific capacitance[11]. Therefore, producing porous carbon from biomass can be a cost-effective and environmentally friendly routine for high-performance EDLCs.

There have been a quite a few reports about the synthesis of biomass derived porous carbon. Ding reported the use of rice husk as a precursor with H_3PO_4 hydrolysis and KOH activation to produce activated carbon with a high surface area of 2156 m^2 g^{-1}[12]. Later, Wang prepared activated carbon by using corncob via a similar process to achieve a higher surface area of 3054 m^2 g^{-1} and a specific capacitance of 401.6 F g^{-1}[13]. Porous carbon can also be synthesized by using various biomass sources, e.g. potato waste residue[14], tapioca[15], bamboo[16], stem bark of broussonetia papyrifera[17] and chestnut shells[18], with a specific surface area of 171.5-2988 m^2 g^{-1} and specific capacitances in the range of 105-495 F g^{-1}. However, there are still a few challenges that limit the production and application of biomass derived porous carbon. For examples, the use of strong acids could be an environment hazard, and the biomass sources such as shiitake mushrooms[19] and willow catkins[20] are either expensive or less abundant. In 2012, Xing reported an activated carbon material from bean dregs, achieving a surface area of 2792 m^2 g^{-1} with KOH activation and exhibiting CO_2 adsorption of up to 4.24 mmol g^{-1}[21]. But the electrochemical properties and pore size distribution of this activated carbon were unclear.

In this paper, we focus on a novel, low-cost (400 USD ton^{-1}) and widely available biomass, bean dregs, which contains 32.5wt% hemicellulose, 20.2wt% cellulose and 0.37wt% lignin, to synthesize porous carbon for supercapacitors. We also explore the effects of different synthetic conditions on the development of pore structure and electrochemical performance. Our method as demonstrated here is facile and can provide cost-effective routines to obtain porous carbon with a high specific surface area (up to 3104 m^2 g^{-1}) and a high specific capacitance (up to 268 F g^{-1}) by KOH activation, yielding superior performance-to-cost ratio. This proposed synthesis method has great potential to be applied to produce porous carbon materials for applications in separation, catalysis and hydrogen storage.

2. EXPERIMENTAL

2.1 Materials

Bean dregs were obtained from China National Cereals, Oils and Foodstuffs Corporation, Lianyungang, Jiangsu Province. The raw bean dreg powders were firstly dried in a blast oven (GZX-

9030MBE, Shanghai Boxun Industrial Co., Ltd. Medical Equipment Factory, China) at 80 °C for 5 h to lower the moisture content to less than 5wt%, grounded into powders (200 mesh) and dried again at 120 °C overnight as the starting material. Elemental analysis was performed on an elemental analyzer (Vario EL III, Elementar, Germany), confirming the weight ratio of elemental C, H, N, S to be 42.07%, 6.41%, 8.40% and 0.48% in the treated bean dregs. All the chemicals, e.g. hydrochloric acid (HCl, 37wt%), hydrofluoric acid (HF, 40wt%), potassium hydroxide (KOH), sulfuric acid (H_2SO_4, 98wt%), ethanol and sodium hydroxide (NaOH) were of analytical grade, purchased from Sinopharm Chemical Reagent Co., Ltd. and used as received.

2.2 Preparation of the porous carbon materials

The raw materials were first carbonized in a high-purity N_2 atmosphere at 400 °C for 0.5 h with a temperature ramping rate of 10 °C min^{-1} and then soaked in 5wt% HCl and 3wt% HF solutions for 6 h each. The obtained powders were repeatedly washed with deionized (DI) water until neutral pH, dried at 80 °C and calcined again at 700-900 °C with KOH at a heating rate of 10 °C min^{-1} under N_2 atmosphere for 1-2 h. KOH was selected as the activator per our preliminary analysis and published results in the literature[12-22]. After activation, the as-prepared samples were immersed in a 5wt% HCl solution for 24 h, washed with DI water until neutral pH and dried at 80 °C. Samples were denoted with the activation temperature, activation ratio (the weight ratio of KOH to the loaded powders, e.g. 2:1 as 2) and activation time (1-2 h). For example, the sample activated at 800 °C with a 4: 1 activation ratio of KOH to the loaded materials for 1 h, was referred to as D-800-4-1.

2.3 Characterization

The morphology of the as-prepared samples was observed by using Cold-Field Scanning Electron Microscopy (SEM) analysis on a Hitachi S-4800 facility with an accelerating voltage of 5 kV. N_2 adsorption-desorption isotherms were obtained on a physical adsorption analyzer (Tristar II 3020, Micromeritics, USA) at -196 °C. The specific surface area and the pore size distribution of the samples were derived from the Brunauer-Emmett-Teller (BET)[23] and Barrett-Joyner-Halenda **(**BJH) methods[24], respectively. X-ray diffraction (XRD) patterns were obtained on an X-ray diffractometer (D/Max 2500v/pc, Rigaku Corporation, Japan) to analyze the crystalline structure of the samples.

2.4 Electrochemical tests

80wt% porous carbon samples were mixed with 10wt% acetylene black and 10wt% polyvinylidene fluoride (PVdF) thoroughly and grounded in the presence of a certain amount of polytetrafluoroethylene (PTFE) and ethanol. The formed slurry was evenly coated on nickel foam substrates (2×1 cm^2). The fabricated electrodes were then maintained under 10 MPa for 3 min and dried again at 80 °C in a vacuum oven. The electrochemical tests were carried out in a three-electrode test cell with 1 M H_2SO_4 solution as the electrolyte. A platinum electrode was used as the counter

electrode and a saturated calomel electrode (SCE) as the reference electrode. Cyclic Voltammetry (CV) was implemented at a scan rate of 50 mV s^{-1} in a potential window of -0.2-0.8 V. Galvanostatic charge and discharge tests were performed at a current density of 1 A g^{-1} in the same potential window. The Electrochemical Impedance Spectroscopy (EIS) analysis was carried out in the frequency range of 0.01 Hz-1000 kHz with an amplitude of 5 mV.

3. RESULTS AND DISCUSSION

It has been confirmed that the activation temperature, time and the amount of activator play a key role in determining the properties of porous carbon[22]. In this paper, we systematically alter these synthetic parameters to study their impacts on the pore structure and electrochemical properties of our prepared porous carbon materials. Fig. 1 shows the SEM images of two typical porous carbon samples D-800-3-1 and D-800-6-1. It is clear that D-800-3-1 (Fig. 1 (a) and (b)) has a relatively smooth surface and possesses massive pores. Under the same activation temperature and time, D-800-6-1 is further etched and more developed and smaller pores appear on its surface, as shown in Fig. 1(c) and (d). We believe the deeper etch on D-800-6-1 is associated with the existence of excess KOH powders during activation.

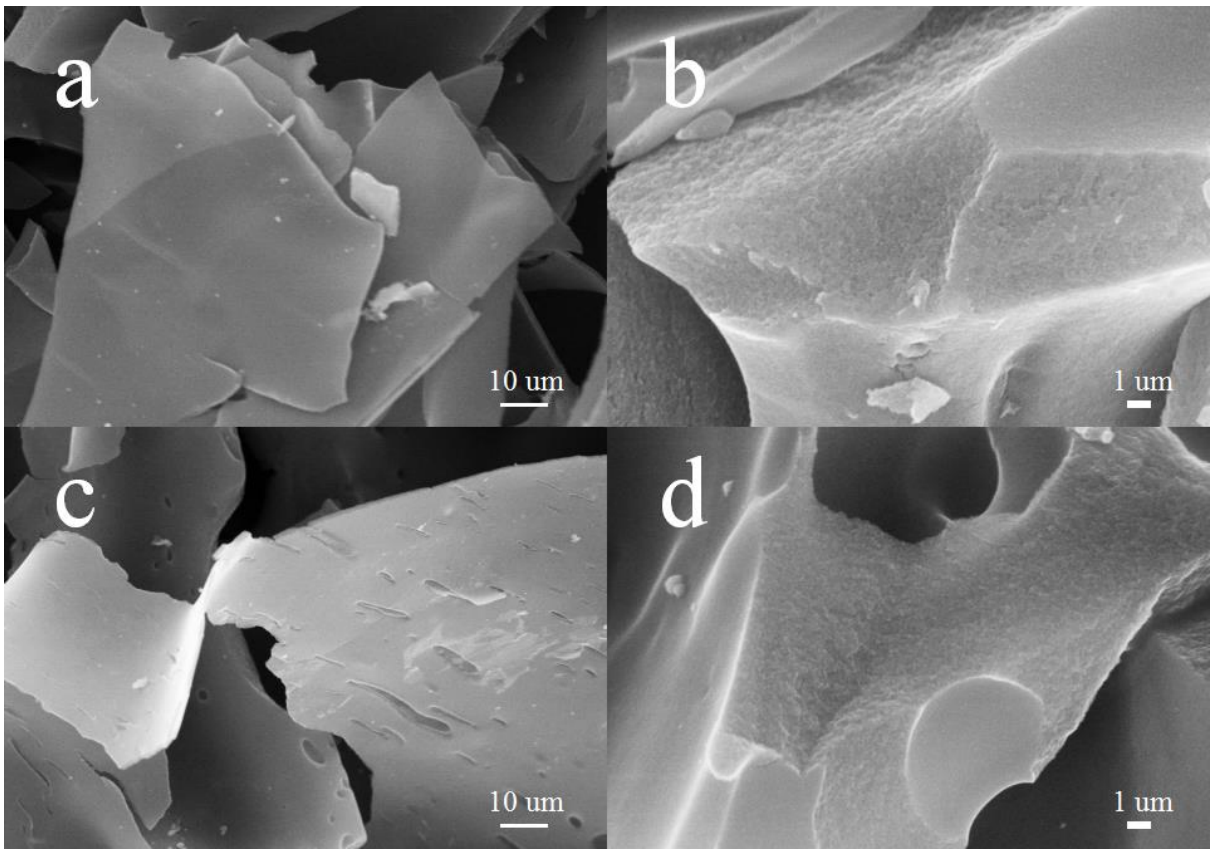

Figure 1. SEM images of samples (a) and (b) D-800-3-1 and (c) and (d) D-800-6-1.

3.1 Activation temperature

All the samples were obtained with the same activation ratio (4: 1) and activation time (1 h), with only the activation temperature varying from 700-900 °C. The electrochemical performance of the as-prepared porous carbon materials was examined as below.

3.1.1 XRD spectrum analysis

Fig. 2 demonstrates the XRD patterns of sample D-700-4-1, D-800-4-1 and D-900-4-1. It can be seen that all the samples show a broad diffraction peak (002) at 23° and another weak peak (100) centered at 45°, indicating amorphous graphitic phases of our porous carbon materials[25].With the increase of temperature, the peak width and graphitization degree of all samples also increase, resulting in reduced resistances as shown in Fig. 4(c).

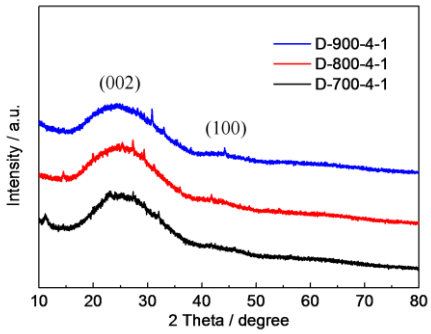

Figure 2. The XRD patterns of D-700-4-1, D-800-4-1 and D-900-4-1.

3.1.2 Pore structure analysis

Fig. 3 shows the N_2 adsorption and desorption isotherms and pore size distribution of samples D-700-4-1, D-800-4-1 and D-900-4-1. The adsorption and desorption isotherm branches of D-700-4-1 are substantially overlapping and can be classified as the Brimauer-Deming-Deming-Teller (BDDT) Type I[26]. At P/P_0=0.3, the adsorption reached its saturation state, indicating quite thorough pore channels without many bottleneck-shaped pores. This type of pore structure is beneficial for the adsorption-desorption of adsorbates[27]. On the other hand, sample D-800-4-1 shows a typical BDDT Type IV isotherms with a significant H4 hysteresis loop at P/P_0=0.4. This indicates clearly that massive mesoporous are embedded within the porous matrix linked by micropores[28]. On the other hand, D-900-4-1 shows the BDDT Type I isotherms, indicating the presence of plenty of micropores and limited mesoporous. The pore size distribution curves in Fig. 3(b) show that all these three porous carbon samples possess dominant mesopores in the size of 3-4 nm. D-800-4-1 shows a quite high volume of mesopores, making a significant contribution to its specific surface area. As seen in Table 1, the specific surface area, total pore volume and mesopore volume increase as the activation temperature rises from 700 °C to 800 °C but decrease when the temperature reaches 900°C. D-800-4-1 adsorbs the most N_2 and has the highest specific surface area (2912 m^2 g^{-1}). The average pore size also

increases with elevated activation temperature and this can be attributed to the reduction of KOH at high temperature and the formation of sublimed metallic potassium (above 762 °C), which diffuse into carbon to create more pores[29].

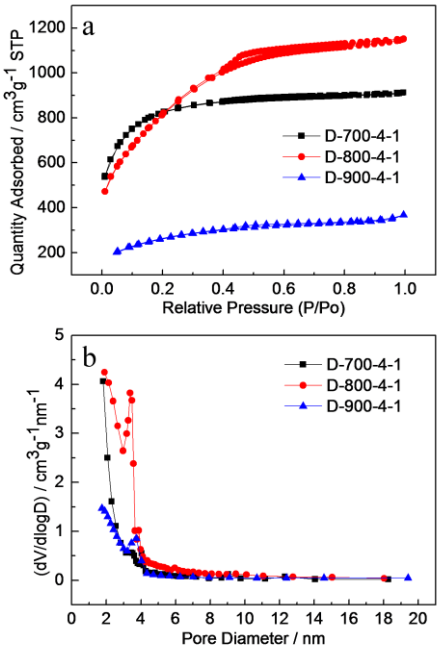

Figure 3. (a) The N_2 adsorption and desorption isotherms and (b) pore size distribution of samples D-700-4-1, D-800-4-1 and D-900-4-1.

Table 1. Texture properties and the specific capacitance of the porous carbons.

Samples	S_{BET}[a] ($m^2\ g^{-1}$)	V_t[b] ($cm^3\ g^{-1}$)	D_{ave}[c] (nm)	V_{mic}[d] ($cm^3\ g^{-1}$)	V_{meso}[e] ($cm^3\ g^{-1}$)	C[f] ($F\ g^{-1}$)
D-700-4-1	2617	1.40	2.15	0.59	0.81	210
D-800-4-1	2912	1.77	2.43	1.14	0.63	215
D-900-4-1	884	0.57	2.57	0.21	0.36	59
D-800-4-1.5	3104	1.89	2.43	1.22	0.67	148
D-800-4-2	2999	1.96	2.61	1.06	0.90	60
D-800-2-1	2869	1.56	2.18	1.13	0.43	175
D-800-3-1	3096	1.77	2.29	1.44	0.33	268
D-800-5-1	2436	1.48	2.43	0.80	0.68	117
D-800-6-1	2128	1.33	2.51	0.60	0.73	177

[a] BET surface area.
[b] Total pore volume.
[c] Average pore diameter.
[d] Micropore volume.
[e] Mesoporous volume.
[f] Special capacitance calculated by CV curves at 50 mVs^{-1}.

3.1.3 Electrochemical Performance

Fig. 4 shows the CV, galvanostatic charge-discharge curves and Nyquist plots of samples D-700-4-1, D-800-4-1 and D-900-4-1. It is clear from Fig. 4(a) that all porous carbon samples obtained at different temperature present a quasi-rectangular shape, indicative of fast charge-discharge capability[30] and typical EDLC behavior[31]. No obvious redox peaks are observed, showing no pseudocapacitance generated by the surface functional groups of these porous carbon samples[22]. Both D-700-4-1 and D-800-4-1 show similar capacitance (210 vs. 215 F g^{-1}) from their CV curves, significantly outperforming sample D-900-4-1 (59 F g^{-1}). We ascribe this to the facilitation of ion diffusion within the large volume of pores in samples D-700-4-1 and D-800-4-1[32]. Furthermore, the galvanostatic charge-discharge curves of all these samples, as shown in Fig. 4(b), demonstrate a similar isosceles triangle shape, also indicating excellent double layer performance[33]. Fig. 4(c) exhibits Nyquist plots of these three samples, all consisting of a semicircle in the high-frequency range and the sloping line in the low-frequency range. The former refers to the charge transfer resistance (R_{ct}); while the latter is the Warburg resistance (Z_w) associated with solid electrode material diffusion. The intercept at the horizontal axis represents the ohmic resistance (R_s) between the electrode surface and the electrolyte[34]. D-900-4-1 shows the smallest semicircle among all three samples, indicating that it has the lowest charge transfer resistance and the best electronic conductivity.

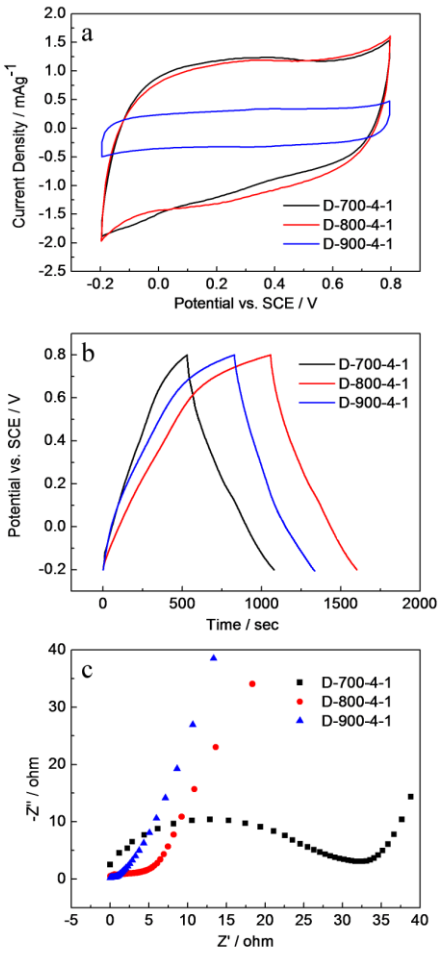

Figure 4. (a) The CV curves, (b) g charge-discharge curves, (c) Nyquist plots of D-700-4-1, D-800-4-1 and D-900-4-1.

3.2 Activation time

All the sample were obtained with the same activation temperature (800 °C) and activation ratio (4: 1), with only the activation time varying from 1-2 h. The electrochemical performance of the as-prepared porous carbon materials was examined as below.

3.2.1 XRD spectrum analysis

From the XRD patterns (Fig. 5), we can see all the samples demonstrate (002) and (100) diffraction peaks, located at 23° and 45°, respectively. The (002) peak is broad and strong while the (100) peak is quite weak. As the activation time increases from 1 to 2 h, the (002) peak becomes broader, suggesting a higher degree of disorder and graphitization which causes reduced resistance (Fig. 7(c)).

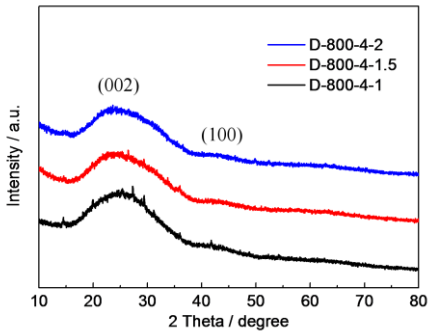

Figure 5. The XRD patterns of D-800-4-1, D-800-4-1.5 and D-800-4-2.

3.2.2 Pore structure analysis

It can be seen from Fig. 6(a) that all samples prepared at different activation time present BDDT Type IV isotherms and at around P/P_0=0.4, an H4 type hysteresis loop is also present indicating the formation of a large number of mesopores within the porous structure. At the activation time of 1.5 h, the highest N_2 adsorption capacity is reached. Fig. 6(b) shows that most of the pores in these samples are in the size of ~4 nm and pore volume increases with the prolonged activation time from 0.36 $cm^3\ g^{-1}$ at 1 h to 0.90 $cm^3\ g^{-1}$ at 2 h. It is also noteworthy that the specific surface area reaches the highest value of 3104 $m^2\ g^{-1}$ when activation lasts for 1.5 h, however, the best capacitance (215 F g^{-1}) of the three sample is obtained at the activation time of 1 h. We believe the high specific surface area does not correlate to the best capacitive performance and the pore size is a key parameter in ion diffusion. Although samples D-800-4-1.5 and D-800-4-2 have slightly higher surface area compared to D-800-4-1, not all their pores are accessible by the ions, therefore, yielding inferior performance[35].

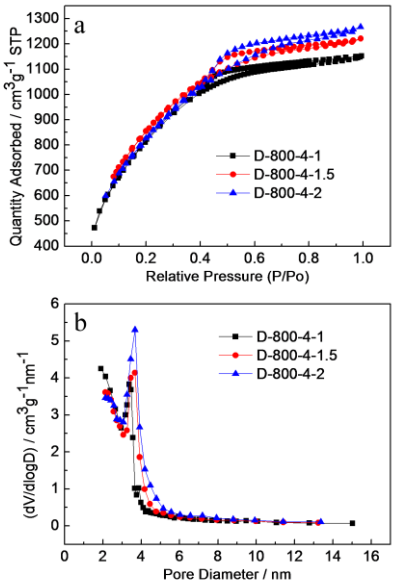

Figure 6. (a) The N_2 adsorption and desorption isotherms and (b) pore size distribution of samples D-800-4-1, D-800-4-1.5 and D-800-4-2.

3.2.3 Electrochemical Performance

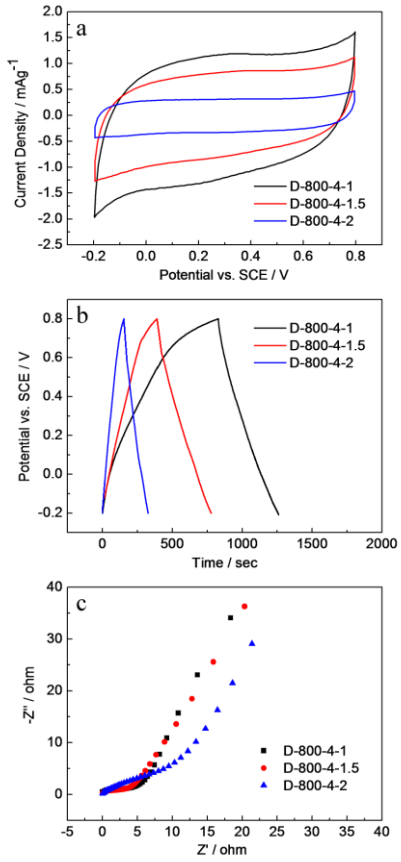

Figure 7. (a) The CV curves, (b) g charge-discharge curves, (c) Nyquist plots of D-800-4-1, D-800-4-1.5 and D-800-4-2.

As seen in Fig. 7(a), all samples prepared at different activation time exhibit a regular rectangular in their CV curves without any redox peaks, suggesting their highly reversible capacitive behaviors[36].Their specific capacitance is 215, 148 and 60 F g^{-1} for samples D-800-4-1, D-800-4-1.5 and D-800-4-2, respectively, as shown in Table 1. And similarly, their galvanostatic charge-discharge curves (Fig. 7(b)) also present an isosceles triangle, reflecting excellent electrochemical double layer characteristics. From the Nyquist plots in Fig. 7(c), we can also observe similar semicircles with associated slopes, referring to charge transfer resistance (R_{ct}) and Warburg impedance (Z_w). Samples D-800-4-1 and D-800-4-1.5 have the lower R_{ct} compared to that of D-800-4-2.

3.3 Activation ratio

All the sample were obtained with the same activation temperature (800 °C) and activation time (1 h), with only the activation ratio varying from 2:1 to 6:1. The electrochemical performance of the as-prepared porous carbon materials was examined as below.

3.3.1 XRD spectrum analysis

Similarly, in Fig. 8, all samples exhibit a broad diffraction peak at 23° and a weak peak (45°), namely (002) and (100) graphitic planes. The (002) peak in D-800-6-1 is much sharper than that of others, indicative of a more crystallized graphite structure which may substantially improve the conductivity of our porous carbon materials. It is well known that alkaline activation results in the formation of a highly porous but disordered structure since KOH tends to attack the aligned (i.e., graphitic) structural domains in the carbon matrix [37]. In the current case, the D-800-6-1 sample shows a relatively higher degree of graphitization probably due to the adequate amount of KOH.

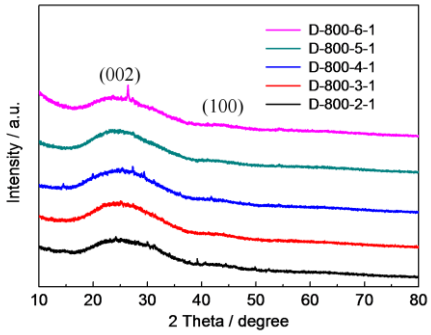

Figure 8. The XRD patterns of D-800-2-1, D-800-3-1 and D-800-4-1, D-800-5-1 and D-800-6-1.

3.3.2 Pore structure analysis

The N_2 adsorption-desorption isotherms of the five examined samples can all be classified as BDDT Type IV (Fig. 9(a)), indicating the presence of a large number of mesopores[38]. The surface area of these samples rises with the activation ratio and reaches the highest value at 3:1 with the largest

pore volume and average pore size (Table 1). Fig. 9(b) shows the pore size distribution curves of all the samples, where the most of the pores lie in the size of 3.5-4.0 nm. We believe that more KOH powders would induce more pores during activation which could lead to the increased surface area. However, an excess amount of KOH will etch the already established pores, further reducing the pore volume and creating open voids.

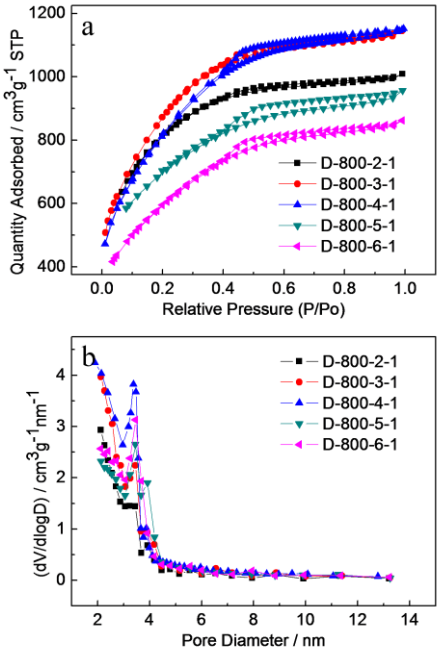

Figure 9. (a) The N_2 adsorption and desorption isotherms and (b) pore size distribution of samples D-800-2-1, D-800-3-1, D-800-4-1, D-800-5-1 and D-800-6-1.

3.3.3 Electrochemical Performance

Similarly, all our porous carbon samples show typical EDLC behavior and D-800-3-1 delivers the highest capacitance of 268 F g^{-1} among all the examined samples (Fig. 10(a)). We also notice a weak reduction peak at -0.1 V for D-800-3-1 and D-800-6-1 and we account it to the C=O groups[39], yielding negligible pseudocapacitance to the overall performance[38-40]. The capacitance reaches the highest at 3:1 because of the highest surface area (3096 m^2 g^{-1}) with highest pore volume (1.77 cm^3 g^{-1}) and the second smallest average pore size (2.29 nm). Fig. 10(b) demonstrates the galvanostatic charge-discharge curves of all examined sample and shows no obvious IR drop, a signature for excellent double layer capacitance[41]. The Nyquist plots in Fig. 10(c) exhibit a similar feature with more obvious semicircles. It can also be seen that the charge resistance gradually decreases along with the increase of the activation ratio. Sample D-800-6-1 has the lowest charge transfer resistance and we credit it to its highly graphitic structure which may produce high electron conductivity[42].

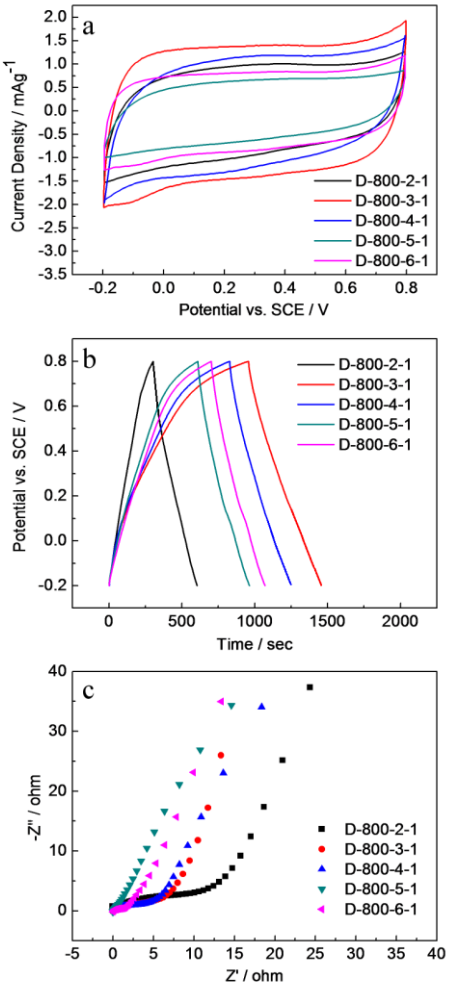

Figure 10. (a) The CV curves, (b) g charge-discharge curves, (c) Nyquist plots of D-800-2-1, D-800-3-1, D-800-4-1, D-800-5-1 and D-800-6-1.

From the above examinations, we believe that activation temperature, time and ratio are all crucial factors affecting the specific surface area, porosity and electrochemical performance of our porous carbon samples. Firstly, activation at high temperature (e.g. 800 °C) can assist in the formation of more developed and accessible mesoporous structure (Fig. 2), improving the specific surface area and specific capacitance, and reducing the internal resistance. However, activation occurring at an even higher temperature (900 °C) may reduce the pore volume (Table 1) by creating more open voids, leading to reduced specific surface area and specific capacitance. Moreover, the pore structure is very sensitive to the activation time. A prolonged activation time will help to increase the total pore volume, but it also increases the pore size and decreases the specific capacitance (Table 1). A reasonable activation time must be discreetly selected to maintain a large total pore volume as well as a large portion of mesopores to maximize the specific surface area and specific capacitance. Additionally, with the same temperature and time, activation with more KOH powders etches more effectively on the sample surface (Fig. 1), however, excess KOH is no longer helpful but over-etches the established pores and drastically decreases the pore volume and specific surface area, yielding poor performance.

Porous carbon prepared from biomass materials have been reported in the literature (Table 2). However, the biomass source was either black fungus, resulting in a lower specific surface area (2233 m^2 g^{-1})[43], or willow catkin and shiitake mushrooms with comparable performance (340 and 306 F g^{-1})[44-45], but through a high-cost and complex routine. In addition, the low availability of willow catkin made it unfavorable for scalable production. Our proposed method in this paper has great potential in commercial gain as we only use an agricultural waste – bean dreg as the source material, and it is also environmentally friendly, eliminating the use of strong acids. Porous carbon derived from our method possesses high surface area and high specific capacitance, indicating promising future commercialization for high-performance supercapacitors via a cost-effective and green approach.

Table 2. Comparison of supercapacitors with similar biomass materials.

Biomass materials	S_{BET} (m^2 g^{-1})	C^f (F g^{-1})	References
corncob	3054	401.6	[13]
potato waste residue	1052	255	[14]
bamboo	171.5	281	[16]
stem bark of broussonetia papyrifera	1538	320	[17]
chestnut shells	1987	105.4	[18]
willow catkins	1507	262	[20]
black fungus	2233	-	[43]
willow catkin	1586	340	[44]
shiitake mushrooms	2988	306	[45]
bean dregs	3104	268.49	This work

4. CONCLUSION

We use low-cost and readily available bean dregs as raw materials to prepare high-performance porous carbon as supercapacitor electrode materials. The as-prepared porous carbon possesses ultrahigh surface area (up to 3104 m^2 g^{-1}) and well-developed pore structure, and its pore structure can be tailored by altering the synthetic conditions in terms of activation temperature, time and ratio. Our best-performing sample (D-800-3-1) can deliver a specific capacitance of 268 F g^{-1}, an indication of superior electrochemical properties for promising EDLCs. The synthetic method and produced porous carbon as demonstrated in this paper can also be applied to other fields such as catalysis and adsorption.

ACKNOWLEDGEMENT
This work was supported by the Prospective joint research projects of production and research of Jiangsu Science and Technology plans (BY 2015027-07, BY 2015027-05).

References

1. A. Magdziarz and M. Wilk, *J. Therm. Anal. Calorim.*, 114 (2013) 519.
2. L.X. Zhang, Z.H. Liu, G.L. Cui and L.Q. Chen, *Prog. Polym. Sci.*, 43 (2015) 136.
3. A. Stein, Z. Wang and M.A. Fierke, *Adv. Mater.*, 21 (2009) 265.
4. D.P. Upare, S. Yoon and C.W. Lee, *Korean J. Chem. Eng.*, 28 (2011) 731.
5. S.J. Yang, H. Jung, T. Kim and R.P. Chong, *Prog. Nat. Sci.*, 22 (2012) 631.
6. M. Michel and B. Buszewski, *Adsorption.*, 15 (2009) 193.
7. G.V. Nunell and M.E. Fernández, *Biomass. Bioenerg.*, 44 (2012) 87.
8. H. Yamada, I. Moriguchi and T. Kudo, *J. Power Sources*, 175 (2008) 651.
9. J.R. Miller and P. Simon, *Sci.*, 321 (2008) 651.
10. L. Zhao, L.Z. Fan, M.Q. Zhou, H. Guan, S. Qiao, M. Antonietti and M.M. Titirici, *Adv. Mater.*, 22 (2010) 5202.
11. M. Sevilla and A.B. Fuertes, *ACS Nano*, 8 (2014) 5069.
12. L.L. Ding, B. Zou, W. Gao, Q. Liu, Z.C. Wang, Y.P. Guo, X.F. Wang and Y.H. Liu, *Colloid Surface. A.*, 446 (2014) 1.
13. D.B. Wang, Z. Geng, B. Li and C.M. Zhang, *Electrochim. Acta*, 173 (2015) 377.
14. G.F. Ma, Q. Yang, K.J. Sun, H. Peng, F.T. Ran, X.L. Zhao and Z.Q. Lei, *Bioresource Technol.*, 197 (2015) 137.
15. M.R. Wang, Y.Q. Lai, J. Fang, J. Li, F.R. Qin, K. Zhang and H. Lu, *Int. J. Hydrogen Energ.*, 40 (2015) 16230.
16. H. Chen, D. Liu, Z.H. Shen, B.F. Bao, S.Y. Zhao and L.M. Wu, *Electrochim. Acta*, 180 (2015) 241.
17. Y.J. Li, G.L. Wang, T. Wei, Z.J. Fan and P. Yan, *Nano Energy*, 19 (2016) 165.
18. L.L. Cheng, P.Z. Guo, R.Y. Wang, L.F. Ming, F.F. Leng, H.L. Li and X.S. Zhao, *Colloid. Surface. A.*, 446 (2014) 127.
19. Y.H. Ma, Q.H. Wang, X.N. Wang, X.H. Sun and X.Q. Wang, *J. Porous Mat.*, 22 (2015) 157.
20. Y.J. Li, N. Yu, P. Yan, Y.G. Li, X.M. Zhou, S.L. Chen, G.L. Wang, T. Wei and Z.J. Fan, *J. Power Sources*, 300 (2015) 309.
21. W. Xing, C. Liu, Z.Y. Zhou, L. Zhang, J. Zhou, S.P. Zhuo, Z.F. Yan, H. Gao, G.Q. Wang and S.Z. Qiao, *Energ. Environ. Sci.*, 5 (2012) 7323.
22. L.L. Ding, B. Zou, H.Q. Liu, Y.M. Li, Z.C. Wang, Y. Su, Y.P. Guo and X.F. Wang, *Chem. Eng. J.*, 225 (2013) 300.
23. G. Pickett, *J. Am. Chem. Soc.*, 67 (2002) 1958.
24. D.W. Li , C.L. Li , Y.Y. Tian , L.Z. Kong and L. Liu, *Mater. Lett.*, 141 (2015) 340.
25. X.M. Ma , M.X. Liu , L.H. Gan , Y.H. Zhao and L.W. Chen, *J. Solid State Electr.*, 17 (2013) 2293.
26. K.S.W. SING, D.H. EVERETT, R.A.W. HAUL, L. MOSCOU, R.A. PIEROTTI, J. ROUQUEROL and T. SIEMIENIEWSKA, *Pure Appl. Chem.*, 57 (1985) 603.
27. W. Hao, E. Björkman, M. Lilliestråle and N. Hedin, *Appl. Energ.*, 112 (2013) 526.
28. J.C. Groen, L.A.A. Peffer and J. Pérez-Ramı'rez, *Micropor. Mesopor. Mat.*, 60 (2003) 1.
29. M. Song, B.S. Jin, R. Xiao, L. Yang, Y.M. Wu, Z.P. Zhong and Y.J. Huang, *Biomass Bioenerg.*, 48 (2013) 250.
30. M.X. Liu, L.H. Gan, W. Xiong, F.Q. Zhao, X.Z. Fan, D.Z. Zhu, Z.J. Xu, Z.X. Hao and L.W. Chen, *Energ. Fuel.*, 27 (2013) 1168.
31. T.E. Rufford, D. Hulicova-Jurcakova, Z. Zhu and G.Q. Lu, *Electrochem. Commun.*, 10 (2008) 1594.
32. W.G. Pell, B.E. Conway and N. Marincic, *J. Electroanal. Chem.*, 491 (2000) 9.
33. D.C. Guo, J. Mi, G.P. Hao, W. Dong, G. Xiong, W.C. Li and A.H. Lu, *Energ. Environ. Sci.*, 6 (2012) 652.
34. J.F. Wu, L. Zuo, Y.H. Song, Y.Q. Chen, R.H. Zhou, S.H. Chen and L. Wang, *J. Alloy. Compd.*, 656 (2016) 745.
35. W.T. Huang, H. Zhang, Y.Q. Huang, W.K. Wang and S.C. Wei, *Carbon*, 49 (2011) 838.

36. S. Yoon, J. Lee, T. Hyeon and S.M. Oh, *J. Electrochem. Soc.*, 147 (2000) 2507.
37. H. Wang, Z. Xu, A. Kohandehghan, Z. Li, K. Cui, X. Tan, T.J. Stephenson, C.K. King'ondu, C.M. Holt and B.C. Olsen, *Acs Nano*, 7 (2013) 5131.
38. W.T. Tsai, H.C. Hsu, T.Y. Su, K.Y. Lin and C.M. Lin, *J. Colloid. Interf. Sci.*, 299 (2006) 513.
39. E. Frackowiak, *Phys. Chem. Chem. Phys.*, 9 (2007) 1774.
40. D. Hulicova-Jurcakova, G. Seredych, G. Q. Lu and T.J. Bandosz, *Carbon*, 46 (2008) 1475.
41. L.L. Ding, B. Zou, L. Shen, C. Zhao, Z.C. Wang, Y.P. Guo, X.F. Wang and Y.H. Liu, *Colloid. Surface. A.*, 446 (2014) 90.
42. T.Y. Wei, X.L. Wei, Y.Gao and H.M. Li, *Electrochim. Acta*, 169 (2015) 186.
43. X.L. Zhang, P.X. Li, R. Zang, S.J. Wang, Y. Zhu, C. Li and G.X. Wang, *Chem. Asian J.*, 12 (2017).
44. W. Kai, Z. Ning, S.W. Lei, R. Yan, X.D. Tian, J.Z. Wang, Y. Song, D.F. Xu, Q.G. Guo and L. Liu, *Electrochim. Acta*, 166 (2015) 1.
45. P. Cheng, S.Y. Gao, P.Y. Zang, X.F. Yang, Y.L. Bai, H. Xu, Z.H. Liu and Z.B. Lei, *Carbon*, 93 (2015) 315.